The Oxidized (**3,3**) State of Manganese Catalase. Comparison of Enzymes from *Thermus thermophilus* and *Lactobacillus plantarum*†

Mei M. Whittaker,‡ Vladimir V. Barynin,§,|| Svetlana V. Antonyuk,|| and James W. Whittaker*,‡

Department of Biochemistry and Molecular Biology, Oregon Graduate Institute of Science and Technology, P.O. Box 91000, Portland, Oregon 97291-1000, Department of Molecular Biology and Biotechnology, University of Sheffield, P.O. Box 594, Firth Court, Western Bank, Sheffield S10 2TN, U.K., and The Institute of Crystallography, Russian Academy of Sciences, Leninsky pr.59, Moscow 117333, Russia

Received March 3, 1999; Revised Manuscript Received May 10, 1999

ABSTRACT: Manganese catalases contain a binuclear manganese cluster that catalyzes the redox dismutation of hydrogen peroxide, interconverting between dimanganese(II) [(**2,2**)] and dimanganese(III) [(**3,3**)] oxidation states during turnover. We have investigated the oxidized (**3,3**) states of the homologous enzymes from *Thermus thermophilus* and *Lactobacillus plantarum* using a combination of optical absorption, CD, MCD, and EPR spectroscopies as sensitive probes of the electronic structure and protein environment for the active site metal clusters. Comparison of results for these two enzymes allows the essential features of the active sites to be recognized and the differences identified. For both enzymes, preparations having the highest catalytic activity have diamagnetic ground states, consistent with the bis-μ-bridging dimanganese core structure that has been defined crystallographically. Oxidative damage and exogenous ligand binding perturb the core structure of LPC, converting the enzyme to a distinct form in which the cluster becomes paramagnetic as a result of altered exchange coupling mediated by the bridging ligands. The TTC cluster does not exhibit this sensitivity to ligand binding, implying a different reactivity for the bridges in that enzyme. A mechanism is proposed involving distinct coordination modes for peroxide substrate in each of the two half-reactions for enzyme turnover.

Antioxidant enzymes such as superoxide dismutase and catalase protect living cells from reactive oxygen species [superoxide, $O_2^{-\bullet}$, and hydrogen peroxide (H_2O_2), respectively] that are responsible for oxidative damage to essential elements of cell structure. Catalases (*1*−*3*) are ubiquitous metalloenzymes that catalyze the redox disproportionation of hydrogen peroxide:

$$2H_2O_2 \rightarrow 2H_2O + O_2 \quad (1)$$

This overall reaction consists of two distinct half-reactions involving alternate reduction and oxidation of the peroxide substrate:

$$\text{reduction, } H_2O_2 \rightarrow [O] + H_2O \quad (2)$$

$$\text{oxidation, } H_2O_2 + [O] \rightarrow O_2 + H_2O \quad (3)$$

One of the oxygen atoms derived from hydrogen peroxide, represented by [O] in these equations, may be retained by the enzyme as it undergoes complementary changes in oxidation and protonation state.

Two major classes of catalase have been characterized, differing in their redox cofactor. The more common heme catalases contain an Fe protoporphyrin IX cofactor (*1*, *4*) which is oxidized by the first molecule of peroxide from a ferric [Fe(III)] heme in the resting enzyme to Compound I, an oxyferryl [Fe(IV)═O] porphyrin π-cation radical (*1*). This high-potential oxidizing species reacts with a second molecule of hydrogen peroxide, being reduced to ferric heme in the process to complete the turnover cycle. When the hydrogen peroxide is depleted at the end of the reaction, half of the catalase molecules can be left in a reactive oxyferryl state, which in some enzymes has been shown to decay via internal electron transfer from a tightly bound NADPH molecule (*5*, *6*).

An alternative, manganese-containing non-heme catalase has been isolated from the thermophilic eubacteria [e.g., *Thermus thermophilus* (*7*, *8*) and *Thermoleophilum album* (*9*)] and from lactic acid bacteria [e.g., *Lactobacillus plantarum* (*10*)]. Crystal structures have been determined for the manganese catalases from *T. thermophilus*[1] (*11*) and *L. plantarum*[2] at high resolution, showing that both enzymes share an unusual catalytic motif, a bridged binuclear man-

† Support for this project from the National Institutes of Health (Grant GM 42680 to J.W.W.) and BBSRC (Grant GRN 50/B05117 to V.V.B.) is gratefully acknowledged.

* Corresponding author. Telephone: (503) 690-1065. Fax: (503) 690-1464. E-mail: jim@bmb.ogi.edu.

‡ Oregon Graduate Institute of Science and Technology.

§ University of Sheffield.

|| Russian Academy of Sciences.

[1] V. V. Barynin, P. D. Hempstead, A. A. Vagin, S. V. Antonyuk, W. R. Melik-Adamyan, V. S. Lamzin, P. M. Harrison, and P. J. Artymiuk, manuscript in preparation.

[2] V. V. Barynin, P. M. Harrison, P. J. Artymiuk, S. V. Antonyuk, V. S. Lamzin, M. M. Whittaker, and J. W. Whittaker, manuscript in preparation.

10.1021/bi990499d CCC: $18.00
Published on Web 06/22/1999

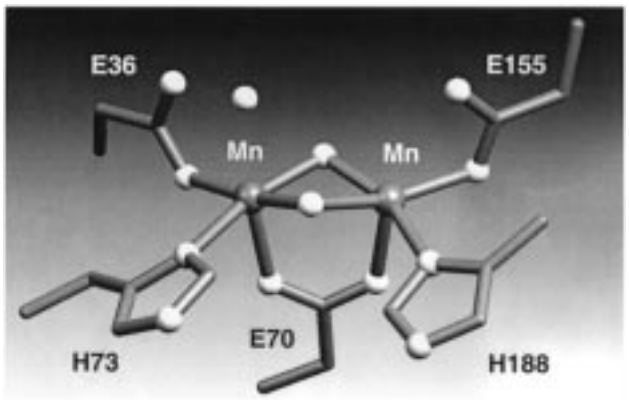

FIGURE 1: Active site of *T. thermophilus* manganese catalase. Heteroatoms (O, N, and Mn) are depicted as spheres (from ref *11*).

Scheme 1

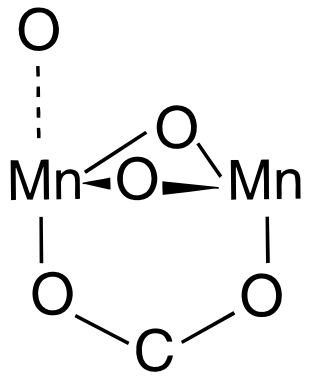

ganese cluster. The structure of the active site of the *T. thermophilus* manganese catalase is shown in Figure 1. The essential features of the catalytic core structures that are conserved between the two enzymes[1,2] are shown in Scheme 1. Bridging oxygens (oxo, hydroxo, or aquo in different cluster oxidation states) support electronic coupling between the metal ions, which are also bridged by a $\mu_{1,3}$-carboxylate ligand. The binuclear Mn active site cycles between [Mn(II)·Mn(II)] [abbreviated as (**2,2**)] and [Mn(III)·Mn(III)] [abbreviated as (**3,3**)] oxidation states during turnover (*12*−*14*). Each of these oxidation states is in principle indefinitely stable, thus making the Mn catalases well suited for protection against the relatively low levels of hydrogen peroxide that challenge microaerophilic species. The active sites can be prepared in multiple oxidation states, including spectroscopically and chemically distinct (**2,2**), (**2,3**), (**3,3**), and (**3,4**) species (*12*, *13*, *15*).

The native manganese catalase enzyme is isolated as a mixture of oxidation states, including (**2,2**), (**3,3**), and minority (**3,4**) species (*12*, *13*, *16*). Studies with the pure (**2,2**) state of LPC, prepared by simple reduction of the resting enzyme, have demonstrated an unusually high affinity for fluoride ions compared to the that of the oxidized (**3,3**) complex (*17*). This reversal of the normal trends in manganese ligand affinity with oxidation state has led to a proposal that the reduced cluster acts as a metallochelate, with substitutional insertion of exogenous ligands into the bridging positions of the cluster core (*17*). Crystallographic data for reduced TTC[3] show that chloride can substitute for one of the oxygen bridges in that complex, supporting this picture of bridge lability in the reduced (**2,2**) state (*11*). Corresponding crystallographic data for pure oxidation states and exogenous ligand complexes of LPC are still lacking. For both enzymes, spectroscopic studies can extend the structural information, revealing electronic features of the active site that relate directly to chemical bonding and molecular reactivity.

Previous studies with the oxidized (**3,3**) state of TTC have shown it to be EPR-silent, consistent with a diamagnetic ground state for the cluster stabilized by the moderately strong antiferromagnetic exchange coupling between high-spin Mn(III) ($S = 2$) metal ions expected for a bis-μ-bridging organization of the dimanganese core (*12*, *15*). In contrast, recent low-temperature MCD studies with the oxidized LPC enzyme prepared by treatment with hydrogen peroxide have defined a ferromagnetically coupled ground state for the oxidized complex, interpreted as evidence for a single μ-bridging hydroxide (*18*). To resolve these issues and to explore the behavior of the oxidized manganese clusters, we have undertaken the first detailed comparison of TTC and LPC (**3,3**) complexes.

MATERIALS AND METHODS

Enzymes. Manganese catalase was isolated from *L. plantarum* (ATCC 14431) as previously described (*10*, *17*, *19*). Manganese catalase was purified from *T. thermophilus* HB8 (ATCC 27634) either as previously described (*12*) or using Chromatofocusing chromatography as described for LPC. Protein concentrations were determined by optical absorption measurements, using the previously reported extinction coefficients [$E^{1\%}_{280} = 10.7$ and $\epsilon_{280} = 3.2 \times 10^4$ M^{-1} cm^{-1} (LPC) (*10*) based on subunit molecular weight (*20*); $E^{1\%}_{280} = 9.5$ and $\epsilon_{280} = 3.4 \times 10^4$ M^{-1} cm^{-1} (TTC) (*20*)]. The metal content of the purified protein was determined by atomic absorption spectrometry. Enzymatic activity was measured by optically detected decomposition of hydrogen peroxide (*10*).

Preparation of Oxidized (3,3) Catalase. Native LPC or TTC was pretreated by incubation with 0.2 M KCl in 50 mM MOPS (pH 6.8) followed by transfer into 50 mM MOPS (pH 7) by dilution−concentration cycles in an Amicon Millipore Centricon-10 ultrafiltration unit to remove exogenous ligands. The protein was titrated under argon with freshly prepared $(NH_2OH)_2 \cdot H_2SO_4$, and the resulting colorless solution was applied to a P-30 size exclusion chromatography column (1.5 cm × 15 cm) equilibrated with 50 mM HEPES (pH 7.5). The reduced, desalted protein was exchanged into 0.1 M TAPS (pH 9) by successive concentration−dilution cycles, diluted to approximately 10 mg/mL in the same buffer, and incubated under an atmosphere of O_2 gas at 4 °C for up to 9 days, resulting in autoxidation to the (**3,3**) state (*12*). Efficient conversion to the (**3,3**) complex requires the protein solution to be maintained at high pH during autoxidation (*12*). The extent of conversion and

[3] Abbreviations: LPC, *L. plantarum* manganese catalase; TTC, *T. thermophilus* manganese catalase; CD, circular dichroism; MCD, magnetic circular dichroism; EPR, electron paramagnetic resonance; EDTA, (ethylenedinitrilo)tetraacetic acid; MOPS, 3-(*N*-morpholino)-propanesulfonic acid; HEPES, *N*-(2-hydroxyethyl)piperazine-*N*′-2-ethanesulfonic acid; TAPS, *N*-tris(hydroxymethyl)methyl-3-aminopropanesulfonic acid.

quantitative extinction coefficients for oxidized complexes of LPC and TTC were determined by direct reductive titration with a standard hydroxylamine solution (see below).

*Reductive Titration of Manganese (**3,3**) Catalase Complexes.* Anaerobic solutions of LPC or TTC (approximately 0.4 mM active sites) were titrated with 10 mM hydroxylamine [as $(NH_2OH)_2 \cdot H_2SO_4$] prepared anaerobically in deionized H_2O, and the progress of the reaction was monitored by recording changes in the visible absorption. The hydroxylamine solution was standardized by titration with Mn(III)EDTA.

Hexachloroiridate Treatment of Mn Catalase. Native LPC [0.625 mM active sites in 50 mM potassium phosphate buffer (pH 7)] was progressively oxidized with Na_2IrCl_6 (20 mM, in H_2O) through aliquot addition up to a 12-fold stoichiometric excess of oxidant. The product was dialyzed against phosphate buffer (pH 7) and exchanged into 50 mM MOPS (pH 7) by repeated concentration−dilution cycles.

Hydrogen Peroxide Treatment of Mn Catalase. Native LPC [0.63 mM active sites in 50 mM potassium phosphate buffer (pH 7)] was dialyzed overnight against 100 mM hydrogen peroxide in the same buffer.

Spectroscopic Measurements. Optical absorption spectra were recorded using a Varian Instruments Cary 5 UV-vis-NIR absorption spectometer interfaced with a microcomputer for data acquisition. Circular dichroism (CD) and magnetic circular dichroism (MCD) spectra were recorded using an AVIV Associates model 40DS UV-vis-NIR dichrometer as previously described (*21*). An Oxford Instruments SM4-6T magnetocryostat provided the magnetic field (0−6 T) and temperature (1.5−300 K) control during MCD spectroscopy. Samples for MCD spectroscopy were prepared as glycerol glasses (approximately 50% glycerol) between quartz disks separated by a silicone rubber spacer (1 or 2.5 mm thick) with a circular bore holding 60 or 120 μL of sample, respectively. Samples were tested for depolarization at low temperatures by comparing spectra for 0.12 M nickel L-(+)-tartarate placed before and after the sample. Low-temperature absorption spectra of LPC and TTC MCD samples was computed from the single-beam transmission data for the sample and a 50% glycerol reference. Electron paramagnetic resonance spectra were recorded on a Varian E-109 X-Band EPR spectrometer equipped with an Air Products helium flow cryostat. Metal ion analyses were performed using a Varian Instruments SpectrAA atomic absorption spectrometer equipped with a GTA 96 graphite furnace for high-sensitivity metal determinations.

RESULTS

*Optical Spectra for Manganese (**3,3**) Catalase.* Oxidized manganese catalase is pink-brown in color as a result of weak absorption in the visible spectrum (Figure 2). TTC and LPC complexes have virtually identical spectra at room temperature with an absorption maximum near 500 nm (475 nm for LPC and 492 nm for TTC) and a broad tail extending into the near IR. Aside from differences in intensity, these spectra are similar to spectra previously reported for the native enzymes (*10*, *12*), since the alternate (**2,2**) oxidation state of the active site lacks any visible absorption. One distinction between the spectra for the two enzymes is a partly resolved near-UV absorption feature, present in the LPC (**3,3**) spectrum near 400 nm, that is absent from the room-temperature spectrum of TTC.

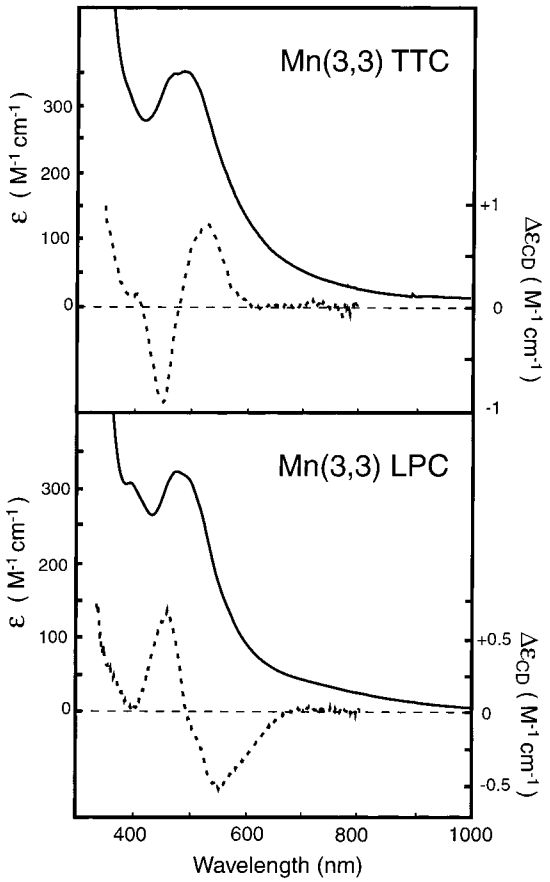

FIGURE 2: Optical spectra for Mn (**3,3**) TTC LPC in 50 mM MOPS buffer (pH 7.0). (Top) (—) Room-temperature absorption spectrum for oxidized TTC (35 mg/mL). (− − −) Circular dichroism spectrum for oxidized TTC. (Bottom) (—) Room-temperature absorption spectrum for oxidized LPC (28 mg/mL). (− − −) Circular dichroism spectrum for oxidized LPC (80 mg/mL). Extinction coefficients were based on the Mn(III) content of the sample determined titrametrically.

The circular dichroism (CD) spectra of the two complexes are also similar, each consisting of a simple, symmetric pattern of nearly equally intense but oppositely signed features centered around the absorption maximum (Figure 2). However, the spectra of the two enzymes are inverted in sign relative to each other, with the positive ellipticity associated with the lower-energy band for TTC and the higher-energy band for LPC. No significant CD intensity is observed beyond 650 nm for either of these complexes. The spectroscopic data are summarized in Table 1.

*Evaluation of the Manganese (**3,3**) Catalase Extinction Coefficient.* Titration of oxidized (**3,3**) LPC or TTC prepared as described in Materials and Methods with a reductant (hydroxylamine) allows the absorption intensity to be directly calibrated in terms of the chemical redox stoichiometry, giving both the value of the visible absorptivity and the extent of conversion to the oxidized complex. For TTC, complete reduction of 0.36 μmol of enzyme (based on active sites) having an initial absorption A_{492} of 0.106 is achieved by reaction with 0.3 μmol of hydroxylamine (Figure 3). On the basis of the two-electron reactivity of the reductant toward the two Mn(III) ions in the oxidized complex (see below), the molar ratio ([NH_2OH]/[active site]) determined from the

Table 1: Spectroscopic Data for Oxidized Manganese Catalases

	ABS[a]		CD		MCD	
	λ (nm)	ϵ (M^{-1} cm^{-1})	λ (nm)	ϵ (M^{-1} cm^{-1})	λ (nm)	ϵ (M^{-1} cm^{-1})
LPC						
290 K	395	310	460	0.72		
	475	330	552	−0.53	−	
4.3 K	400	380	340	−2.5	−	
	490	390	400	−0.4		
	625		465	2		
			525	−2.5		
LPC and F^-						
	505	385	390	0.6	350	−11
			457	0.7	420	20
			600	−0.7	495	−12
					520	3.7
					545	−1.7
					570	0.4
					605	−1.6
					700	1
LPC and $IrCl_6^{2-}$						
	478	1100			345	−5
					447	11
					545	−6.5
TTC						
290 K	492	360	452	−1.1	−	
			530	0.8		
4.3 K	455	390	327	6	−	
	515		395	1.7		
	625		445	−3.1		
			505	3.7		
TTC and F^-						
	510	370	340	0.6	−	
			440	−0.3		
			520	0.7		
			600	−0.2		

[a] Extinction values quoted here have not been corrected for protein scattering (approximately 15% of the reported value; see the text for details).

titration (0.84 ± 0.05) represents the fraction of the (**3,3**) complex present in this autoxidized sample, from which the extinction coefficient may be calculated (ϵ_{492} = 358 M^{-1} cm^{-1}). This sample was converted by a relatively brief (overnight) incubation under O_2, and we have found that longer incubation of TTC (9 days) leads to complete conversion to the (**3,3**) form. Similar analysis of a sample of autoxidized LPC indicated quantitative conversion to the (**3,3**) form (1.02 ± 0.05) and a visible extinction coefficient close to that found for TTC (ϵ_{475} = 327 M^{-1} cm^{-1}). In the concentrated samples required for these absorption measurements, the protein scattering tail makes a significant contribution to the visible spectrum, amounting to approximately 15% of the initial absorption of these complexes. Thus, the actual absorptivity associated with the (**3,3**) active site is correspondingly lower than estimated above, with corrected values for ϵ_{492} of 300 M^{-1} cm^{-1} for TTC and for ϵ_{475} of 296 M^{-1} cm^{-1} for LPC for the Mn(III)-specific absorption. Biochemical characterization of samples prepared in this fashion demonstrates that their catalytic activity (38 000 units/mg for TTC and 8800 units/mg for LPC) equals or exceeds the maximum reported specific activity for these enzymes.

EPR spectroscopy was used to further characterize the reaction of manganese catalase with hydroxylamine and to establish the equivalence ratio for reduction (Figure 4). The oxidized complex lacks significant EPR intensity aside from the relatively strong multiline absorption near $g = 2$ arising

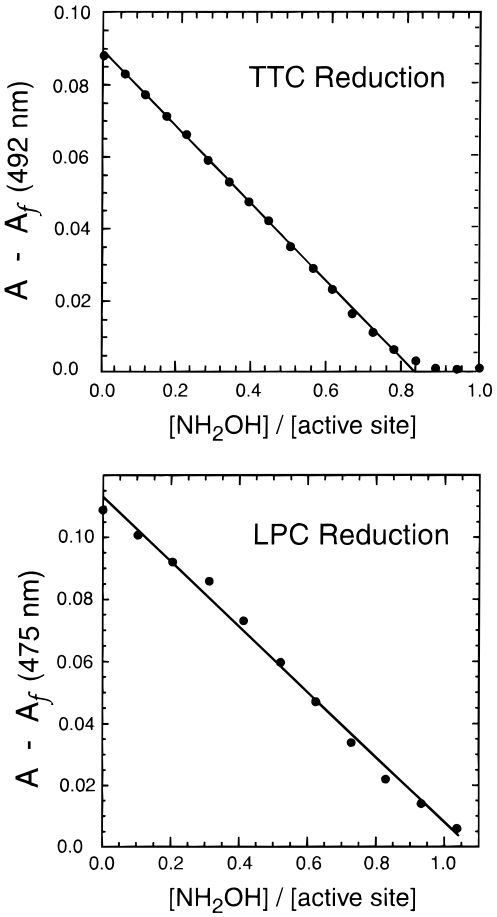

FIGURE 3: Stoichiometric redox titration of Mn (**3,3**) catalase absorption spectra for quantitation of the oxidized complex. (Top) TTC [13 mg/mL in 50 mM MOPS buffer (pH 7.0)] under argon was titrated with aliquot addition of an anaerobic aqueous solution of $(NH_2OH)_2 \cdot H_2SO_4$ (20 mM in hydroxylamine), monitoring progress in the reaction by the change in absorbance at 492 nm. (Bottom) LPC [11.6 mg/mL in 50 mM MOPS buffer (pH 7.0)] under argon was similarly titrated with aliquot addition of an anaerobic aqueous solution of $(NH_2OH)_2 \cdot H_2SO_4$ (20 mM in hydroxylamine), monitoring the progress of the reaction at 475 nm. The lines drawn in each panel are linear least-squares fits to the data.

from a minority mixed-valent (**3,4**) species, amounting to less than 10% of the enzyme sample based on EPR spectral integration and activity measurements (*12*) (Figure 4A). Addition of 0.9 stoichiometric equivalent of hydroxylamine leads to a dramatic increase in the intensity of EPR resonances at both lower and higher fields, identified from earlier work as the spectrum of the reduced (**2,2**) catalase (Figure 4B). Addition of an excess (1.8 equiv) of hydroxylamine (Figure 4C) leads to only a slight further increase in this signal.

Polarization Spectroscopy. CD and MCD spectra for oxidized manganese catalase at low temperatures (4.3 K) in a glycerol glass are shown in Figure 5. Both TTC (Figure 5, top) and LPC (Figure 5, bottom) exhibit a significant enhancement in rotational strength at low temperatures, associated with a sharpening and a slight shift in energy of the CD bands (Table 1), but retain the approximate inversion symmetry between spectra for the two enzymes. Application of a magnetic field induces weak circular polarization [magnetic circular dichroism (MCD)] signals in both of these samples, shown in the insets of Figure 5. However, the

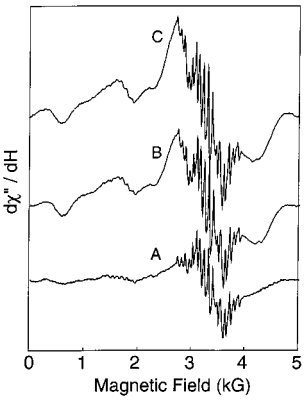

FIGURE 4: EPR spectra for LPC complexes. (A) LPC (**3,3**) catalase [1 mM active sites in 50 mM MOPS (pH 7)], (B) LPC (**3,3**) catalase [1 mM active sites in 50 mM MOPS (pH 7)] and 0.9 mM NH_2OH, and (C) LPC (**3,3**) catalase [1 mM active sites in 50 mM MOPS (pH 7)] and 1.8 mM NH_2OH. Instrumental parameters were as follows: frequency, 9.340 GHz; modulation amplitude, 10 G; modulation frequency, 100 kHz; microwave power, 5 mW; temperature, 20 K.

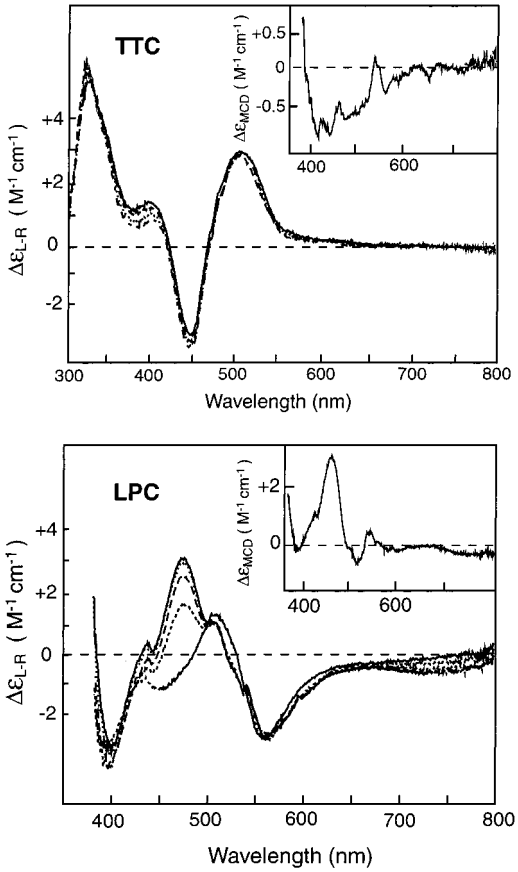

FIGURE 5: MCD data for Mn (**3,3**) TTC and LPC. (Top) Oxidized TTC [1.67 mM active sites, 20 mM MOPS (pH 7), and 60% glycerol glass, with a 2.5 mm path at 4.3 K]. Magnetic field *H* of 0 (—), 1 (- - -), 2 (- — -), and 3 T (•••). (Inset) MCD spectrum (4 T). (Bottom) Oxidized LPC [2.05 mM active sites, 25 mM MOPS (pH 7), and 50% glycerol glass, with a 1.0 mm path at 4.3 K]. Magnetic field *H* of 0 (—), 1 (- - -), 2 (- — -), and 3 T (•••). (Inset) MCD spectrum (4 T). Extinction coefficients ($\Delta\epsilon$) are based on the Mn(III) content of the sample determined titrametrically.

intensity of the magnetic field-dependent component of the spectra is small, comparable to or weaker than the CD spectra which represent the zero field baseline for MCD measurements. The absorption spectra of these same samples (Figure 6) are significantly sharpened at cryogenic temperatures but retain the same basic features seen in the room-temperature absorption spectra (Figure 2), with partial resolution of a low-energy shoulder near 600 nm for both TTC and LPC and a remarkable sharpening of the near-UV feature in the LPC spectrum (400 nm).

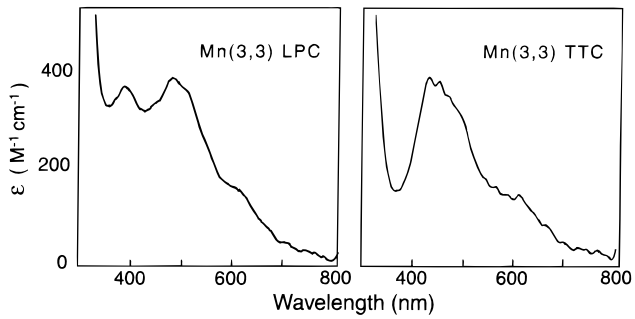

FIGURE 6: Low-temperature absorption spectra for oxidized Mn catalase complexes: (left) Mn (**3,3**) LPC and (right) Mn (**3,3**) TTC. Sample parameters are as indicated in the legend of Figure 5.

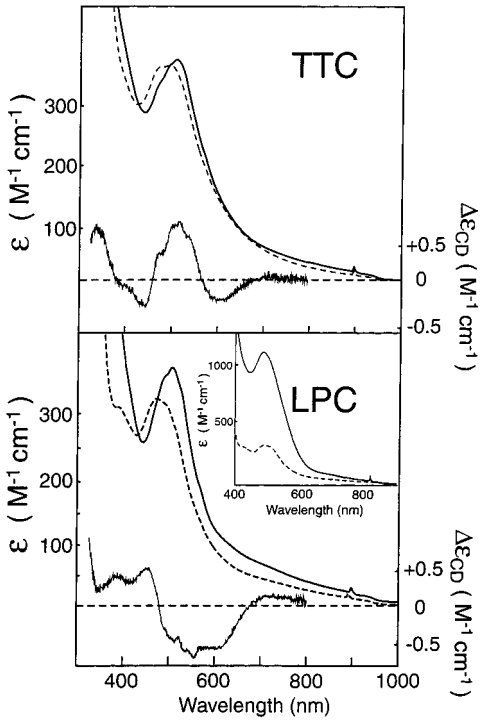

FIGURE 7: Absorption and CD spectra for fluoride complexes of TTC and LPC. (Top) (- - -) Absorption spectra for the TTC (**3,3**) complex [1 mM active sites in 50 mM MOPS (pH 7.0)] and (—) the complex and 200 mM KF and the CD spectrum of the fluoride complex (right-hand intensity scale). (Bottom) (- - -) Absorption spectra for the LPC (**3,3**) complex [1 mM sites in 50 mM MOPS (pH 7)] and (—) the complex and 200 mM KF and the CD spectrum of the fluoride complex (right-hand intensity scale). (Inset) (- - -) Absorption spectra for the LPC (**3,3**) complex [1 mM active sites in 50 mM MOPS (pH 7)] and (—) the absorption spectrum for Ir(IV)-treated LPC [0.13 mM active sites in 50 mM MOPS (pH 7)].

Treating LPC with a powerful oxidant [hexachloroiridate (Na_2IrCl_6)] results in a dramatic increase in the intensity of the visible absorption without a significant shift in the absorption maximum (Figure 7, bottom, inset). The absorptivity (ϵ_{478}) of the enzyme rises to at least 1140 M^{-1} cm^{-1} in this complex, assuming quantitative conversion. However, a lower level of conversion cannot be excluded, and the sample may represent a mixture of native (**3,3**) and modified

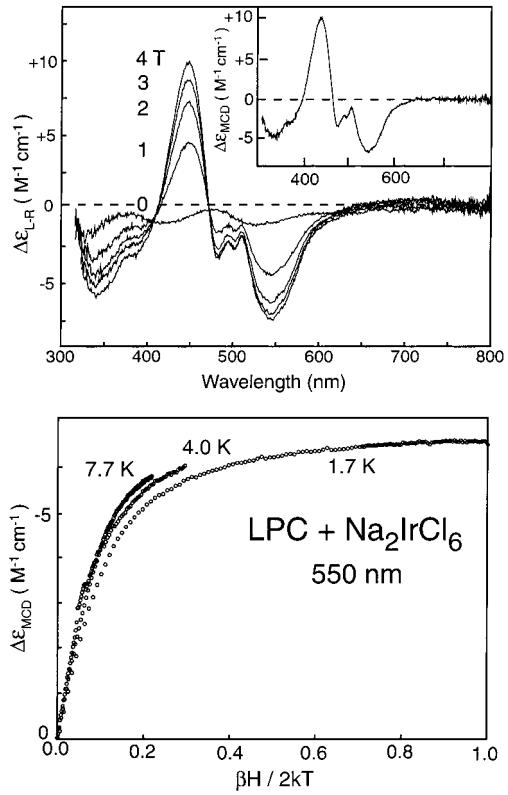

FIGURE 8: MCD data for hexachloroiridate-treated LPC. (Top) Zero field CD baseline and spectra recorded with variable magnetic fields (1−4 T) at 4.3 K. (Inset) MCD spectrum (4 T). (Bottom) Saturation magnetization profiles for low-temperature (1.7−7.7 K) variable-magnetic field (0−5 T) MCD.

complexes, making the extinction value quoted above a lower limit. The catalytic activity of the Ir(IV)-treated enzyme is substantially reduced (5600 units/mg, approximately 60%) compared to that of the native enzyme as isolated, before addition of oxidant, and metal ion analyses indicate that 10% of the Mn has been lost as a result of this treatment. This sample exhibits low-temperature MCD with intensities at high magnetic fields approaching 10 times the amplitude of the underlying CD baseline. The pattern of MCD intensity includes a negatively signed band in the near UV (at approximately 350 nm), a positively signed band (near 450 nm), and a negatively signed band near 550 nm. All three features appear to exhibit similar saturation behavior (Figure 8, top), and the magnetization of MCD in the 550 nm band between 1.7 and 7.7 K is described in more detail in the lower panel of Figure 8. A slope−intercept analysis (*22*) of the saturation profile at the lowest temperature (1.7 K) is consistent with an axial ground-state Zeeman factor $g_{||}$ of 9 associated with the magnetization behavior. The same analysis applied to the saturation profile for the high-spin mononuclear pentachloromanganate(III) $[MnCl_5]^{2-}$ complex [data not shown (*21*)] leads to an estimate for $g_{||}$ of 10 in the ground state. Although it has been previously reported that peroxide treatment results in the appearance of intense optical absorption features in the visible spectrum (ϵ_{476} = 2500 M^{-1} cm^{-1}) (*18*), we find that treatment of LPC with hydrogen peroxide has no appreciable effect on the optical absorption spectrum when starting from the mixed oxidation state of the native enzyme.

Fluoride Complexes. Addition of fluoride to the (**3,3**) sites leads to a shift of the absorption to lower energy for both

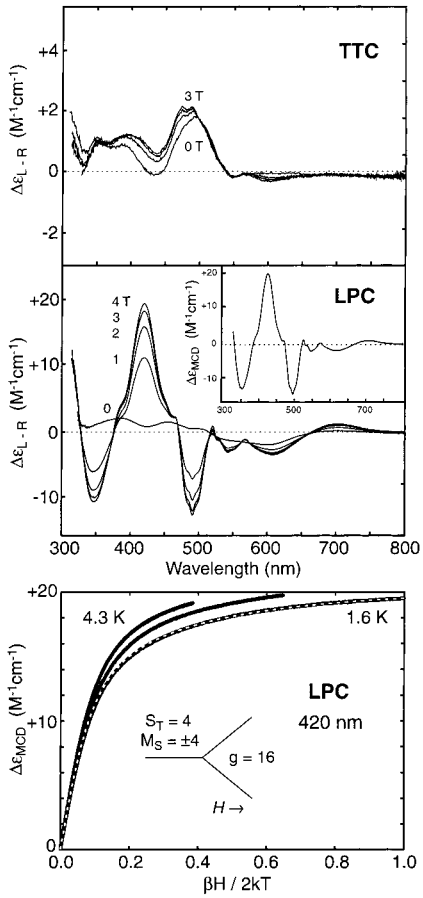

FIGURE 9: MCD data for manganese catalase fluoride complexes. (Top) TTC [1.67 mM active sites in 20 mM MOPS (pH 7) and 60% glycerol] with 200 mM KF. Spectra recorded for low-temperature (4.3 K) variable-magnetic field (0−3 T) MCD. (Middle) LPC [2.78 mM active sites in 25 mM MOPS (pH 7) and 50% glycerol] with 200 mM KF. Spectra recorded for low-temperature (4.3 K) variable-magnetic field (0−4 T) MCD. (Inset) MCD spectrum (4 T). (Bottom) Saturation magnetization profiles for LPC and KF for variable-temperature (1.6−4.3 K) variable-magnetic field (0−5 T) MCD. (- - -) Simulation of the magnetization profile at 1.6 K based on the polarization model with a g = 16 ground-state Zeeman splitting as described in the text.

LPC and TTC (Figure 7), with a slight increase in absorption intensity. The CD spectra for these complexes are considerably more complex than those recorded for the native (**3,3**) state, with at least four bands resolved across the visible spectrum. The fluoride complex of TTC lacks any appreciable MCD intensity (Figure 9, top) at low temperatures with magnetic fields of up to 3 T. In contrast, the LPC fluoride complex exhibits intense MCD across the entire UV−vis region with significant intensity extending into the near IR, resolving at least eight distinct components between 300 and 800 nm. The MCD amplitude approaches 20 times the underlying CD intensity in the strongest features, with a saturation limit intensity of 20 M^{-1} cm^{-1} at 420 nm. The saturation behavior of the LPC fluoride MCD spectra is shown in Figure 9 (bottom) for temperatures between 1.6 and 4.3 K. The lowest-temperature saturation magnetization curve analyzed in terms of a mixed polarization model (*23*) based on a ground-state g value of 16 yields the following polarization components: m_{xy} = 20 and m_z/m_{xy} = −2.

EPR spectra for fluoride complexes of both LPC and TTC (**3,3**) catalases are shown in Figure 10. The TTC complex

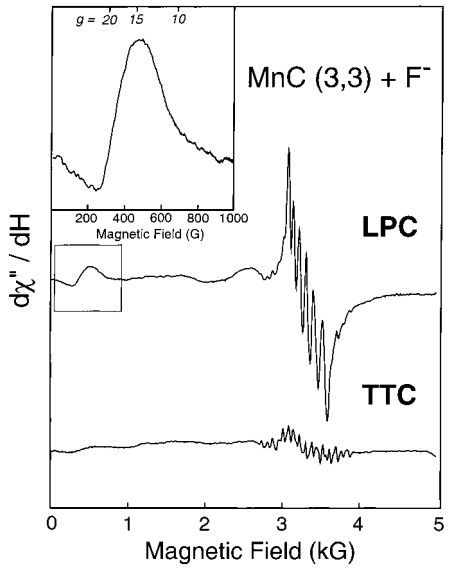

FIGURE 10: EPR spectra for manganese catalase fluoride complexes. (Top) LPC (1 mM active sites in 50 mM MOPS pH 7, 200 mM KF). (Bottom) TTC [1 mM active sites in 50 mM MOPS (pH 7) and 200 mM KF]. The boxed region at low field in the LPC (**3,3**) fluoride spectrum is expanded in the inset. Instrumental parameters were as follows: frequency, 9.340 GHz; modulation amplitude, 10 G; modulation frequency, 100 kHz; microwave power, 5 mW; gain, 1.25×10^4; temperature, 9 K.

exhibits only weak resonance absorption over the entire magnetic field range shown at X-band. For LPC, in addition to strong absorption from mononuclear Mn(II) near the free electron *g* value (at 3340 G), there are additional resonances extending to low field, with a relatively intense feature near $g = 15$ that is enlarged in the inset. The intensity of this feature increases as the temperature is lowered below 15 K.

DISCUSSION

Manganese catalases have been the focus of recent work resulting from comparative analysis of heme catalases, possible chemical analogies with the tetramanganese cluster identified as the water-splitting active site in the photosystem II oxygen-evolving complex, and correlations with binuclear iron systems. The emerging high-resolution structures for the active sites of TTC and LPC give these biochemical and spectroscopic studies a new dimension, and permit a detailed correlation between structures and reactivity for remotely related biological clusters. In these studies, the catalytically important (**2,2**) and (**3,3**) oxidation states are of special interest.

The accessibility of multiple-cluster oxidation states makes the spectroscopic detection and quantitation of these forms in a mixture a special challenge in these studies. While both the fully reduced (**2,2**) complex and the mixed valent (**3,4**) oxidized dimanganese cluster give rise to distinctive EPR spectra at low temperatures, the absence of any EPR signature for the oxidized (**3,3**) form makes its quantitation more problematic. In earlier studies, the fraction of the (**3,3**) form was typically estimated by subtracting the sum of alternative species from the total (*12*). We have found that a combination of optical spectroscopies (absorption, CD, and MCD) provide quantitative probes of this catalytically important complex that are useful in characterizing cluster interactions.

The reduced (**2,2**) TTC autoxidizes under O_2, allowing efficient preparation of the (**3,3**) complex (*12*). The same approach may be used to prepare the (**3,3**) complex of LPC, and although autoxidation of reduced LPC is significantly slower, both enzymes are essentially quantitatively converted to the oxidized form after reaction for 10 days at basic pH. The observation that LPC autoxidizes at a substantially slower rate than TTC is consistent with structural differences. In particular, the channel that penetrates the protein and provides access to the active site is wider in TTC than in LPC.[2] The absorption and CD spectra of the oxidized complexes shown in Figure 2 have been calibrated by redox titration which establishes the extent of conversion and also defines the absorptivity of these complexes.

The titrant used in this analysis must be a reductant that reacts efficiently with the complex and for which the redox stoichiometry is known. Hydroxylamine has been used extensively to reduce manganese catalase (*12*−*17*, *24*), but the reduction ratio does not appear to have been previously measured. The EPR evidence shown in Figure 4 indicates that hydroxylamine acts as a two-electron reductant toward the binuclear Mn(III) cluster in manganese catalase, and on the basis of this reduction ratio, we have been able to determine both the extent of conversion and the absorptivity of the oxidized complexes. The overall reaction is analogous to the well-characterized reduction of Fe(III) by this reagent (*25*), which implies the following formulation that is characteristic of the reaction of hydroxylamine with Mn(III) under alkaline conditions (*26*):

$$NH_2OH + 2Mn(III) \rightarrow {}^1/_2N_2O + {}^1/_2H_2O + 2Mn(II) \quad (4)$$

At lower pH, this reaction is typically replaced by single-electron reactivity (*26*):

$$2NH_2OH + 2Mn(III) \rightarrow N_2 + 2H_2O + 2H^+ + 2Mn(II) \quad (5)$$

The two-electron reaction with the enzyme may reflect an overall basic environment in the active site or may simply be a proximity effect, the second Mn(III) ion reacting with the initially formed $NH_2O^\bullet$ radical before it can diffuse out of the active site. Since hydroxylamine is itself susceptible to autoxidation in the presence of O_2 (*27*), the reductions were performed under an inert atmosphere to ensure accurate quantitation of Mn(III) in the protein samples.

On the basis of this method, the autoxidized LPC and TTC samples whose analyses are depicted in Figure 3 contain 100 and 84% (**3,3**) complex, respectively. In other experiments, we have fully converted TTC simply by extending the oxygen incubation time. The high specific activity of these enzyme samples (which increases during the course of the conversion process, probably as a result of elimination of catalytically inactive species during reduction) attests to the quality of these preparations. The A_{280}/A_{450} absorption ratio calculated for the homogeneous (**3,3**) complexes (109 for TTC and 93 for LPC) permits estimation of the fraction of the (**3,3**) form in the freshly isolated native enzyme. We find that the extent of conversion is variable but consistently high in our preparations of LPC, with up to 90% conversion to the (**3,3**) state [although the actual amount will be lower if other absorbing species, e.g., the (**3,4**) form, are also present].

The extent of conversion in particular samples may reflect culture conditions or the method of purification.

Extinction coefficients calculated for the (**3,3**) complexes in this way on calibrated redox stoichiometry are significantly lower than those reported recently, but our results are consistent with earlier estimates for TTC (*12*). The lower values found here [approximately 150 M^{-1} cm^{-1} per Mn(III) ion] are characteristic of six-coordinate roughly octahedral inorganic complexes such as Mn(III)EDTA (*28*), rather than low-symmetry five-coordinate complexes such as found in Mn(III)SOD for which larger extinction values [approximately 850 M^{-1} cm^{-1} per Mn(III) ion] are more typical (*21*). Although up to four spin-allowed ligand field transitions may in principle occur for each Mn(III) ion and thus as many as eight distinct transitions for a pair of Mn(III) ions, the approximate reflection symmetry relating the two Mn ions in the cluster (Figure 1) significantly reduces the number of resolved features in the spectra of the manganese catalases. Taken together, these results imply effective six coordination for both metal ions in the dimanganese cluster, with similar environments for both subsites. However, each of these clusters is clearly distinct, and the low-temperature absorption spectra for LPC and TTC (Figure 6) reflect significant differences in coordination for Mn(III) in the two proteins.

CD spectra for the two manganese catalases (Figure 2) further emphasize both similarities and differences between the two enzymes. The strong CD associated with the (**3,3**) cluster gives rise to a strikingly simple spectrum, a symmetric pair of features with equal and oppositely signed ellipticities. This spectrum is distinct from that previously reported (*18*), in particular lacking a lower-energy feature near 690 nm. The simpler spectra that we observe are reminiscent of excitonic CD induced by a torsion between degenerate interacting transition dipoles (*29*). However, inspection of the active site (Figure 1) does not reveal any obvious structural basis for an exciton coupling mechanism for the polarization. The reversal in sign between CD spectra for (**3,3**) TTC and (**3,3**) LPC further suggests that the two complexes are effectively enantiomeric, but again the origin of this effect is not clear from the structures. The Mn subsites within the clusters are related by an approximate mirror symmetry plane that bisects the Mn−Mn vector in TTC (*10*) (Figure 1). Exact mirror symmetry would eliminate any intrinsic CD for the dimanganese core, and the experimentally observed strong CD (Figure 2) implies that a symmetry-breaking perturbation must be present to make the two subsites nonequivalent. The perturbation might involve preferential solvation (aquation) of one of the metal centers, or chelation of one subsite by a nonbridging carboxylate. Either of these alterations would introduce dissymmetry into the cluster and shift energies for corresponding transitions in the two subsites, giving rise to oppositely signed CD bands, the metal centers resolving into a pair of oppositely handed chromophores. The approximate inversion symmetry between CD spectra for TTC and LPC implies that a similar perturbation may occur on opposite subsites in the two enzymes. As a point of reference, the strongest CD band in the spectrum of the mononuclear manganese site in Mn(III)SOD is assigned to a spin-allowed ligand field transition with carboxylate → Mn(III) ligand-to-metal charge-transfer character (*30*), further implicating the carboxylate ligands in the unusual CD spectra of Mn (**3,3**) catalase complexes.

Weak magnetic circular dichroism signals are observed for both samples at low temperatures. The MCD spectra observed for TTC occur predominantly in the near-UV region, with features characteristic of the (**3,4**) cluster oxidation state (*31*) but with lower intensity, consistent with a minority fraction of the protein occurring in that form. No additional features are resolved over the lower-energy range corresponding to the visible absorption features of the (**3,3**) complex. For (**3,3**) LPC, a distinct MCD spectrum is observed that resembles features previously identified as arising from the native (resting) (**3,3**) cluster (*18*), but again with lower intensity, the signal shown in Figure 5 being approximately 5-fold lower than previously reported. It is evident that the MCD observed for these autoxidized samples arise from minority paramagnetic components which dominate the spectra only because of the special sensitivity of MCD spectroscopy to paramagnetic species and the fact that the majority of the sample is diamagnetic and therefore not active in MCD. The spectrum observed for the LPC sample is distinct from that found for the (**3,4**) complex, perhaps reflecting the presence of mononuclear or uncoupled Mn(III) centers corresponding to the uncoupled or monomeric Mn(II) previously detected in the reduced (**2,2**) complex (*17*). The low-temperature visible absorption spectra of LPC and TTC resemble cryogenic spectra of six-coordinate Mn(III)SOD anion complexes (*32*), consistent with the crystallographic data.

Treating native enzyme with hexachloroiridate increases the visible absorption intensity with only a slight shift in transition energy (Figure 7 bottom, inset), but with a substantial (nearly 50%) loss of catalytic activity. After this treatment, the overall absorption spectrum is still characteristic of Mn(III) complexes, but the increase in intensity implies a structural change that relaxes parity selection rules for ligand field (d → d) absorption, such as lowering coordination number or eliminating approximate inversion symmetry elements in the complex by removing trans ligand interactions. Loss of one of the metal ions or displacement of a metal ligand would be expected to have this effect. Since the Ir(IV)-treated enzyme retains most of its Mn content, the latter explanation seems more likely, suggesting that one of the oxygen bridges may be lost in this complex. The strong, temperature-dependent MCD associated with the hexachloroiridate-treated enzyme (Figure 8, top) implies a paramagnetic ground state for the cluster in this form, rather than the diamagnetic ground state stabilized in the active (**3,3**) complex. The saturation of the MCD signal observed for this complex (Figure 8, bottom) leads to an estimate for $g_{||}$ of 9 by the slope−intercept method (*22*), intermediate between the magnitude expected for mononuclear Mn(III) ($g_{||} = 8$) and a pair of ferromagnetically coupled Mn(III) ions ($g_{||} = 16$) (see below). Thus, the signals may arise from uncoupled or monomeric Mn(III) centers, since polarization effects can raise the apparent g value evaluated by this method (*23*), and we find that a well-characterized Mn(III) monomeric complex ($[MnCl_5]^{2-}$) gives rise to very similar MCD saturation curves (*21*), with an even larger estimate for the ground-state g value ($g_{||} = 10$). On the other hand, the observed pattern of MCD intensity is very similar to that found for the fluoride complex of LPC (Figure 9) where the evidence for a ferromagnetic ground state is more convincing (see below). Because of its relatively low specific activity,

we believe that this paramagnetic derivative is an artifact of the oxidant-damaged enzyme rather than a catalytically relevant species, and in any case may represent only a minority of the enzyme complexes. These results demonstrate that while the active (**3,3**) manganese catalase has a diamagnetic ground state and consequently lacks paramagnetic MCD, it is possible to convert the cluster to a paramagnetic form by damaging the protein or by coordinating anions (see below). Our observation that hydrogen peroxide does not significantly affect the optical absorption spectrum of LPC further shows that the strongly absorbing species reported previously (*18*) is not a "pulsed" form of the enzyme resulting from modification of the resting enzyme under turnover conditions. There is no evidence that treating Mn catalase with its substrate, hydrogen peroxide, results in the type of oxidative damage associated with Ir(IV) treatment, characterized by the formation of a paramagnetic (**3,3**) complex. Thus, the observation of a paramagnetic ground state for the (**3,3**) form of H_2O_2-treated LPC in a previous MCD study (*18*) must be a consequence of other aspects of sample preparation or sample history.

Binding fluoride converts both TTC and LPC to anion complexes with distinct optical absorption and CD spectra (Figure 7). The approximate inversion symmetry between CD spectra for LPC and TTC complexes persists in these complexes, although less accurately than in the resting (**3,3**) complex. Although the optical and CD spectra are similar for LPC and TTC fluoride complexes, the MCD spectra are very different. In the presence of fluoride, LPC exhibits strong paramagnetic MCD, with a saturation intensity ratio ($\Delta\epsilon_{MCD}/\epsilon_{ABS} = 0.05$) comparable to that found for Mn(III)-SOD complexes (*21*) [approximately 0.05 for both native (five-coordinate) and anion-bound (six-coordinate) complexes] (Figure 9, middle). To the extent that $\Delta\epsilon_{MCD}/\epsilon_{ABS}$ reflects the Faraday ratio $C°/D°$ between the intrinsic parameters determining the temperature-dependent paramagnetic C-Term MCD intensity ($C°$) and the dipole strength of the absorption ($D°$) (*33*), its value might be expected to be fairly constant for ions with similar values for spin−orbit coupling and covalency such as Mn(III) centers in related complexes. The relatively low value of $\Delta\epsilon_{MCD}/\epsilon_{ABS}$ found for the native ($\Delta\epsilon_{MCD}/\epsilon_{ABS} = 0.01$) and hexachloroiridate-treated complexes ($\Delta\epsilon_{MCD}/\epsilon_{ABS} = 0.01$) could then be viewed as an indication that the paramagnetic sites giving rise to the MCD signals represent at best a minority species in the sample. TTC lacks any significant low-temperature MCD intensity in this complex, suggesting that its binuclear complex retains a diamagnetic ground state in the fluoride adduct (Figure 9, top).

The striking saturation behavior of the LPC fluoride complex (Figure 9, bottom) cannot be accounted for in terms of an isolated $S = 2$ ground state for a monomeric Mn(III) ion, and is more consistent with a high-spin ground state associated with an electronically coupled binuclear complex. Saturation of the MCD signal implies a ground-state Zeeman splitting that is large compared to the thermal energy, kT ($\approx$3 cm^{-1} at 4.3 K). This Zeeman splitting within a pair of doublet sublevels is given by

$$\Delta E_{ZEE} = g_{eff}\beta H \quad (6)$$

where g_{eff} is the effective g value, β is the electronic Bohr magneton, and H is the magnetic field strength. The principal components of the effective **g** tensor within a doublet may be evaluated as follows (*34*):

$$g_i = 2g_0\langle S_i\rangle = 4\langle S_i\rangle \quad (7)$$

where g_0 is the intrinsic g value (=2.00) and i is the coordinate index (x,y,z). For Zeeman interactions (βH) that are small compared to ground-state zero field splittings, eq 7 predicts a large effective axial g value ($g_{||} = 16$) within the $M_S = \pm 4$ doublet of an $S_T = 4$ ground state for a pair of ferromagnetically coupled high-spin Mn(III) ions while a much smaller g value ($g_{||} = 8$) is predicted for the $M_S = \pm 2$ non-Kramers doublet of an $S = 2$ ground state associated with an isolated Mn(III) ion. The relatively large Zeeman effect within an $M_S = \pm 4$ doublet ground state can account for the strong saturation of MCD at low magnetic fields ($g_{||}\beta H = 15$ cm^{-1} at 2 T), and the nesting of magnetization curves implies near degeneracy for the non-Kramers doublet. EPR spectroscopy provides a complementary probe that supports this picture of a paramagnetic ground state for the LPC fluoride complex (Figure 10). The low-field EPR absorption near $g = 15$ is distinct from the spectra observed for the reduced manganese catalase fluoride complex (*17*), and this signal grows in intensity at cryogenic temperatures, indicating that it arises within the lowest sublevels of the ground state, again consistent with a nearly degenerate $M_S = \pm 4$ non-Kramers doublet of a ferromagnetically coupled dimanganese(III) cluster ($g_{||} \approx 16$) with small rhombic splitting. Ferromagnetic ground states are stabilized in binuclear complexes of manganese and iron when the antiferromagnetic contributions to electronic exchange are decreased by geometric or electronic factors. For example, when bridging M−O−M bond angles approach 90°, the orthogonality of valence p-orbitals in the bridge σ-coupling pathway eliminates a dominant contribution to antiferromagnetic exchange and results in ferromagnetic or weak antiferromagnetic interactions between the metal ions. Stabilization of valence orbitals on the bridging atoms by protonation has a similar effect (*35*−*37*). Reduced antiferromagnetic coupling may also result from displacement of a bridging atom labilized by fluoride binding, or substitutional insertion of fluoride into the bridge position. The spectroscopic data reported here are consistent with all of these structural models.

Our observations give insight into aspects of the coordination chemistry of the dimanganese active site in manganese catalase that are relevant to catalysis. To set the stage for a discussion of these mechanistic implications, Scheme 2 illustrates important biological iron−peroxide complexes that can serve as models for catalytic intermediates in manganese catalase. Hemerythrin is an invertebrate oxygen-carrier protein containing a binuclear iron cluster that reversibly binds dioxygen as hydroperoxide. Spectroscopic and crystallographic studies have shown that the hydroperoxide molecule is bound terminally in this complex, and is reducing toward the coupled binuclear Fe cluster, which is converted from the [Fe(III)·Fe(III)] state to the [Fe(II)·Fe(II)] state during oxidation of peroxide to O_2, with the oxo bridge being protonated (hydroxo) in this process (*38*). The peroxide oxidation step in manganese catalase catalysis (eq 3) similarly requires reduction of the oxidized (**3,3**) catalase by substrate

Scheme 2

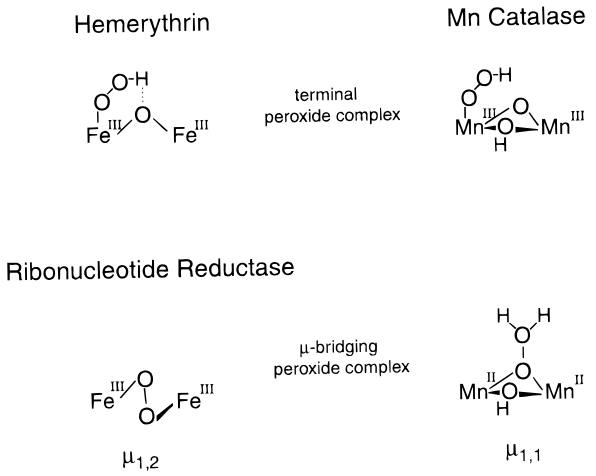

and elimination of the O_2 product, suggesting a strong analogy with hemerythrin coordination chemistry in this step. The terminally bound peroxide shown in Scheme 2 in the active site of Mn catalase correlates into an end-on bound dioxygen on oxidation, facilitating dissociation of the product. In fact, terminal coordination of exogenous ligands in the (**3,3**) state appears to be favored on the basis of the spectroscopic data reported previously (*17*) and extended here. Protonation of the bridges in anion adducts may provide an explanation for the stabilization of a ferromagnetic ground state in the LPC fluoride complex and suggest a role for the bridging ligands as proton acceptor sites in this reaction.

The peroxy intermediate of ribonucleotide reductase is an effective model for the cluster oxidation half-reaction that leads to reduction of the peroxide substrate by manganese catalases (eq 2). The primary oxidative intermediate (compound X) involved in the activation of the ribonucleotide reductase R2 subunit has recently been shown by resonance Raman spectroscopy to consist of a binuclear ferric cluster with $\mu_{1,2}$ bridging peroxide (*39*) (Scheme 2). The $\mu_{1,2}$ bridging mode for peroxide coordination in this high-potential oxy species is particularly favorable for homolytic bond cleavage and free radical reactions (*40*), well-suited to the biological function of this active site, the free radical oxidation of a tyrosyl side chain to a phenoxyl radical. In the catalase reaction, on the other hand, heterolytic rather than homolytic O−O bond cleavage is most likely to occur, avoiding the creation of free radical intermediates. Heterolytic peroxide cleavage is favored by the polarization of the O−O bond that occurs in the $\mu_{1,1}$ bridging mode, shown for the *gem*-protonation isomer of hydrogen peroxide in Scheme 2. Isomerization of hydrogen peroxide contributes to the bond polarization, and a similar peroxide isomerization step has been proposed to occur in the mechanism of heme-containing peroxidases (*41*). From these considerations, it seems likely that the catalytic active site of manganese catalase interacts with peroxide in distinct coordination modes in each of the half-reactions.

On the basis of the available experimental evidence for bridge lability and exchange in the reduced (**2,2**) cluster contrasting with relatively weak anion interactions characteristic of nonbridging coordination modes in the (**3,3**) complex, a mechanism for catalytic turnover is proposed in Scheme 3. Substrate peroxide binds to the oxidized (**3,3**)

Scheme 3

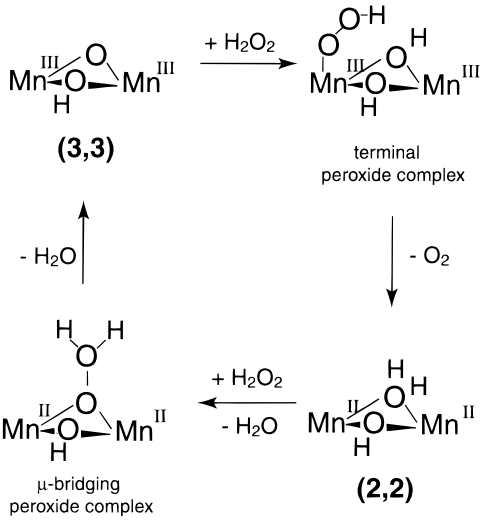

cluster as a terminal ligand and reduces the cluster in a two-electron step that forms a weakly coordinating terminal dioxygen as the product. The lability of the bridging groups in the (**2,2**) state will allow substitutional insertion of peroxide into a bridging position of the reduced complex in forming a $\mu_{1,1}$ hydroperoxy intermediate. In analogy to the heme-containing peroxidases, residues in the active site may catalyze the isomerization of peroxide to the *gem*-protonation isomer, further polarizing the O−O bond for heterolytic bond cleavage (*42*). This proposal leads to a number of experimentally verifiable predictions that are the focus of current studies.

CONCLUSION

The oxidized (**3,3**) state of manganese catalases have diamagnetic ground states in their resting states, associated with a bis-μ-bridged dimanganese core structure. Active sites damaged by treatment with oxidants are converted to paramagnetic species that may contain uncoupled Mn(III) centers or may exhibit ferromagnetic exchange coupling within the modified cluster. Fluoride binding to the oxidized (**3,3**) dimanganese cluster of LPC perturbs the electronic coupling within the cluster ground state, giving rise to clear signatures of a ferromagnetically coupled $S_T = 4$ ground state for the cluster in both MCD and EPR spectra. The same complex of TTC retains a diamagnetic ground state, indicating that the ligand perturbation responsible for the altered ground-state properties of the fluoride adduct of LPC may not reflect mechanistically important consequences of exogenous ligand interactions. Despite the obvious similarities between the *Thermus* and *Lactobacillus* manganese catalases, this first direct comparison of the two enzymes has revealed clear differences in the spectra (reflecting structural differences) and reactivity (including the strikingly different autoxidation rates and the sensitivity of the cluster ground state to exogenous ligands). These insights support a mechanism involving distinct ligation modes (terminal or bridging) for substrate interactions with the redox active dimanganese core in the oxidative and reductive half-reactions.

REFERENCES

1. Schonbaum, G. R., and Chance, B. (1976) in *The Enzymes* (Boyer, P. D., Ed.) 3rd ed., Vol. XIII, Part C, pp 363−408, Academic Press, New York.

2. Vainshtein, B. K., Melik-Adamyan, W. R., Barynin, V. V., and Vagin, A. A. (1984) in *Progress in Bioorganic Chemistry and Molecular Biology* (Ovchinnikov, Yu. A., Ed.) pp 117−126, Elsevier, New York.
3. Beyer, W. F., Jr., and Fridovich, I. (1988) *Basic Life Sci. 49*, 651−661.
4. Melik-Adamyan, W. R., Barynin, V. V., Vagin, A. A., Borisov, V. V., Vainshtein, B. K., Fita, I., Murthy, M. R. N., and Rossmann, M. G. (1986) *J. Mol. Biol. 188*, 63−72.
5. Bicout, D. J., Field, M. J., Gouet, P., and Jouve, H. M. (1995) *Biochim. Biophys. Acta 1252*, 172−176.
6. Ivanovich, A., Jouve, H. M., and Gaillard, J. (1997) *Biochemistry 36*, 9356−9364.
7. Barynin, V. V., and Grebenko, A. I. (1986) *Dokl. Akad. Nauk SSSR 286*, 461−464.
8. Barynin, V. V., Vagin, A. A., Melik-Adamyan, W. R., Grebenko, A. I., Khangulov, S. V., Popov, A. N., Adnrianova, M. E., and Vainshtein, B. K. (1986) *Sov. Phys. Dokl. 31*, 457−459.
9. Allgood, G. S., and Perry, J. J. (1986) *J. Bacteriol. 168*, 563−567.
10. Kono, Y., and Fridovich, I. (1983) *J. Biol. Chem. 258*, 6015−6019.
11. Barynin, V. V., Hempstead, P. D., Vagin, A. A., Antonyuk, S. V., Melik-Adamyan, W. R., Lamzin, V. S., Harrison, P. M., and Artymiuk, P. J. (1997) *J. Inorg. Biochem. 67*, 196.
12. Khangulov, S. V., Barynin, V. V., and Antonyuk-Barynina, S. V. (1990) *Biochim. Biophys. Acta 1020*, 25−33.
13. Waldo, G. S., Fronko, R. M., and Penner-Hahn, J. E. (1991) *Biochemistry 30*, 10486−10490.
14. Waldo, G. S., and Penner-Hahn, J. E. (1995) *Biochemistry 34*, 1507−1512.
15. Khangulov, S. V., Barynin, V. V., Voevodskaya, N. V., and Grebenko, A. I. (1990) *Biochim. Biophys. Acta 1020*, 305−310.
16. Fronko, R. M., and Penner-Hahn, J. E. (1988) *J. Am. Chem. Soc. 110*, 7554−7555.
17. Meier, A., Whittaker, M. M., and Whittaker, J. W. (1996) *Biochemistry 35*, 348−360.
18. Brunold, T. C., Gamelin, D. R., Stemmler, T. L., Mandal, S. K., Armstrong, W. H., Penner-Hahn, J. E., and Solomon, E. I. (1998) *J. Am. Chem. Soc. 120*, 8724−8738.
19. Beyer, W. F., Jr., and Fridovich, I. (1985) *Biochemistry 24*, 6460−6467.
20. Igarashi, T., Kono, Y., and Tanaka, K. (1996) *J. Biol. Chem. 271*, 29521−29524.
21. Whittaker, J. W., and Whittaker, M. M. (1991) *J. Am. Chem. Soc. 113*, 5528−5540.
22. Thomson, A. J., and Johnson, M. K. (1980) *Biochem. J. 191*, 411−420.
23. Bennett, D. E., and Johnson, M. K. (1987) *Biochim. Biophys. Acta 911*, 71−80.
24. Khangulov, S. V., Goldfeld, M. G., Gerasimenko, V. V., Andreeva, N. E., Barynin, V. V., and Grebenko, A. I. (1990) *J. Inorg. Biochem. 40*, 279−290.
25. Bengtsson, G. (1973) *Acta Chem. Scand. 27*, 1717−1724.
26. Salem, I. A. (1995) *Transition Met. Chem. 20*, 312−315.
27. Moews, P. C., Jr., and Audrieth, L. F. (1959) *J. Inorg. Nucl. Chem. 11*, 242−246.
28. Hamm, R. E., and Suwyn, M. A. (1967) *Inorg. Chem. 6*, 139−145.
29. Charney, E. (1985) *The Molecular Basis of Optical Activity*, R. E. Krieger Publishing Co., Malabar, FL.
30. Whittaker, M. M., Ekberg, C. A., Edwards, R. A., Baker, E. N., Jameson, G. B., and Whittaker, J. W. (1998) *J. Phys. Chem. B 102*, 4668−4677.
31. Gamelin, D. R., Kirk, M. L., Stemmler, T. L., Samudranil, P., Armstrong, W. H., Penner-Hahn, J. E., and Solomon, E. I. (1994) *J. Am. Chem. Soc. 116*, 2392−2399.
32. Whittaker, M. M., and Whittaker, J. W. (1996) *Biochemistry 35*, 6762−6770.
33. Piepho, S. B., and Schatz, P. (1983) *Group Theory in Spectroscopy with Applications to Magnetic Circular Dichroism*, Wiley, New York.
34. Huynh, B. H., and Kent, T. A. (1983) in *Advances in Mossbauer Spectroscopy* (Thosar, B. V., Srivastava, J. K., Iyengar, P. K., and Bhargava, S. C., Eds.) pp 490−560, Elsevier Scientific Publishing Co., New York.
35. Blondin, G., and Girerd, J.-J. (1990) *Chem. Rev. 90*, 1359−1376.
36. Hotzelmann, R., Wieghart, K., Flörke, U., Haupt, H.-J., Weatherburn, D. C., Bonvoison, J., Blondin, G., and Girerd, J.-J. (1992) *J. Am. Chem. Soc. 114*, 1681−1696.
37. Gorun, S. M., and Lippard, S. J. (1991) *Inorg. Chem. 30*, 1625−1630.
38. Sanders-Loehr, J. (1988) *Prog. Clin. Biol. Res. 274*, 193−209.
39. Moënne-Loccoz, P., Baldwin, J., Ley, B. A., Loehr, T. M., and Bollinger, J. M., Jr. (1998) *Biochemistry 37*, 14659−14663.
40. Yoshizawa, K., Ohta, T., Yamabe, T., and Hoffmann, R. (1997) *J. Am. Chem. Soc. 119*, 12311−12321.
41. Poulos, T. L., and Kraut, J. (1980) *J. Biol. Chem. 255*, 8199−8205.
42. Bosch, E., Lluch, J. M., and Bertrán, J. (1990) *Can. J. Chem. 68*, 666−673.

BI990499D